

TRANSFER OF AURORAL KILOMETRIC RADIATION THROUGH LOW-DENSITY CHANNELS AT THE BOUNDARY OF PLASMASPHERE

V.I. Kolpak

*Pushkov Institute of Terrestrial Magnetism, Ionosphere,
and Radio Wave Propagation RAS,
Troitsk, Moscow, Russia, lera.kolpak@yandex.ru
National Research University Higher School of Economics,
Moscow, Russia*

M.M. Mogilevsky

*Space Research Institute of RAS,
Moscow, Russia, mogilevsky2012@gmail.com*

D.V. Chugunin

*Space Research Institute of RAS,
Moscow, Russia, dimokch@mail.ru*

A.A. Chernyshov

*Space Research Institute of RAS,
Moscow, Russia, achernyshov@iki.rssi.ru*

I.L. Moiseenko

*Space Research Institute of RAS,
Moscow, Russia, moiseenko.irene@gmail.com*

Abstract. We present the results of Auroral Kilometric Radiation (AKR) measurements near the plasmapause on the ERG (Arase) satellite. The apogee of the satellite's orbit is located near the ecliptic plane, at latitudes $\pm 30^\circ$. According to the generally accepted point of view, AKR observation is impossible in this region since it is shielded by the plasmasphere. Simultaneous measurements of AKR and local plasma density made it possible to determine that AKR in near-equatorial regions occur in plasma channels — density inhomogeneities elongated along magnetic field lines. AKR from sources located in the auroral magnetosphere is transferred by these channels to the equatorial region. This work analyzes the conditions for the capture and

propagation of AKR in low plasma density channels. In the geometrical optics approximation, we have simulated the conditions for the radiation capture and propagation. The calculation results show that the proposed scheme for AKR capture into plasma channels can explain the measurement results — the radiation transfer from the auroral region to the near-equatorial region.

Keywords: auroral kilometric radiation, radiation capture into the channel, plasma inhomogeneities, artificial Earth satellite, space experiment, upper hybrid resonance frequency.

INTRODUCTION

The paper analyzes propagation of auroral kilometric radiation (AKR) in an inhomogeneous plasma at the outer boundary of the plasmasphere. AKR, first recorded by the Electron-2 satellite [Benediktov et al., 1965], represents the most intense natural radiation of Earth's magnetosphere. Subsequent measurements carried out on various spacecraft made it possible to determine the basic features and characteristics of AKR, as well as the conditions for its generation [Wu, Lee, 1979; Gurnett, 1974; Hanasz et al., 2003; Kurth et al., 1975; Xiao et al., 2022; Zhao et al., 2019; Mogilevsky et al., 2007; Chernyshov et al., 2022a; Chugunin et al., 2020; Baumjohann, Treumann, 2022]. AKR arises from the development of cyclotron maser instability in auroral regions of the magnetosphere in cavities with low plasma density [Wu, Lee, 1979], where the following condition holds

$$f_{pe} < f_{Be}, \quad (1)$$

where f_{pe} and f_{Be} are the electron plasma frequency and gyrofrequency respectively.

According to the theoretical model of AKR generation [Wu, Lee, 1979], the major portion of the radiation is a right-handed polarized extraordinary mode, which is

generated near the local electron gyrofrequency. In the source, in plasma without boundaries, the main part of the radiation energy flux is directed across the magnetic field, but walls of the cavity make up a waveguide that determines the AKR distribution along the magnetic field [Louarn, Le Quéau, 1996; Burinskaya, Rosh, 2007]. Walls of the waveguide can also be the boundaries of the flux of superthermal electrons producing radiation energy [Burinskaya, Rosh, 2007].

From ISEE-1 satellite measurements it was first found that AKR can propagate through plasma channels [Calvert, 1982] outside the radiation generation region. Mogilevsky et al. [2022], using ERG satellite (Arase) data, have shown that plasma inhomogeneities elongated along the magnetic field can contribute to the AKR capture into the plasma channel, which causes the radiation spectrum to transform during its propagation in this channel. Yet, it is still unclear under what physical conditions in near-Earth space AKR is captured into plasma channels and propagates in them.

According to the generally accepted point of view [Wu, Lee, 1979], AKR sources are located at heights 3–10 thousand km in the auroral region, and the radiation cone centered on the magnetic field direction in the radiation region has a size $\pm(25^\circ-35^\circ)$ [Mogilevsky et al., 2007]. An extraordinary right-handed polarized elec-

tromagnetic wave propagates from Earth and is reflected from the plasmapause. Thus, AKR from sources in the Northern Hemisphere cannot be recorded in the Southern Hemisphere, and vice versa. Nonetheless, in some cases, AKR from sources located in one hemisphere can be observed in the other hemisphere [Chernyshov et al., 2022b; Kolpak et al., 2021]. To explain this phenomenon, a theory has been developed (see, e.g., [Wu, 1985]) according to which not only the RX mode is generated in the AKR source, but also the Z mode whose intensity is much lower and therefore can hardly be seen near the source. However, the Z mode passes through the plasmasphere to the opposite hemisphere, where it can be detected.

We use AKR data obtained by the Japanese ERG (Exploration of energization and Radiation in Geospace) satellite in the near-equatorial region of Earth's magnetosphere on L -shells ~ 4 – 6 . The satellite's orbit has an apogee of 32000 km and a perigee of 400 km; the orbital inclination is 31° , the orbital period is 570 min [Miyoshi et al., 2018a, b]. Plasma and electromagnetic field parameters are measured using a complex of scientific equipment including receivers in various frequency ranges, as well as detectors of particles and plasma parameters in a wide range of energies [Nagai et al., 2018]. This work relies on measurements of the electric field components with HFA (High-Frequency Analyzer) included in PWE [Kumamoto et al., 2018; Kasahara et al., 2018]. HFA is designed to measure the electric field and plasma waves in a frequency range from 2 kHz to 10 MHz.

In this paper, we discuss the possibility of AKR transfer between the hemispheres as a result of radiation capture into the channels formed near the plasmapause by plasma inhomogeneities elongated along the magnetic field. We analyze the conditions for the radiation capture into plasma channels and its propagation in these channels from one hemisphere to another, using results of ERG (Arase) satellite measurements and modeling in the geometrical optics approximation.

MEASUREMENT RESULTS

For the analysis, we have chosen two measurement intervals in March 2019 and December 2018. The top panel of Figure 1 displays a dynamic spectrogram constructed from measurements of the strength of the electromagnetic field electric component perpendicular to the axis of the satellite rotation. The rotation axis is sunward. The bottom panel presents a spectrogram of the parameter P ($P \in [-1...+1]$), which can conditionally be called polarization. This parameter is described in [Kumamoto et al., 2018; Mogilevsky et al., 2022]. The ERG (Arase) satellite rotates around the direction to the Sun with an orbital period of 8 s. The P parameter is the projection of wave polarization onto a plane perpendicular to the satellite's rotation axis. When observing radiation from sources in the auroral region in the nightside magnetosphere, this parameter fits the classical definition of polarization, i.e. the direction of electric vector rotation in the electromagnetic wave field. In the case of observation of sources from the daytime magnetosphere, this parameter acquires the opposite sign. In the dawn and dusk sec-

tors of the magnetosphere, P vanishes (which corresponds to linear polarization or its absence) even for waves with circular polarization due to the coincidence of the plane of polarization with the plane perpendicular to the direction to the Sun.

The underline presents the satellite's orbital parameters along the orbit: UT — universal time; MLT — magnetic local time; MLAT — geomagnetic latitude; R — distance to the satellite in Earth radii; z_{sm} is the z coordinate in the SM (Solar-Magnetic) coordinate system.

There is a narrowband signal in the low-frequency part of the spectrogram, which varies from 100 to 200 kHz. These are variations in the electric-field component at the upper hybrid resonance frequency

$$f_{\text{hrp}} = (f_{\text{pe}}^2 + f_{\text{Be}}^2)^{1/2}, \quad (2)$$

where f_{pe} is the local electron plasma frequency:

$f_{\text{pe}} = (4\pi e^2 N / m_e)^{1/2}$ (in the SGS system); e is the electron charge; N is the plasma density; m_e is the electron mass; f_{Be} is the local electron gyrofrequency: $f_{\text{Be}} = eB / m_e c$; B is magnetic induction; c is the velocity of light.

The electron gyrofrequency f_{Be} in this region varies from a few kilohertz to 10 kHz, and so we can assume with good accuracy that the upper hybrid resonance frequency f_{uhr} depends mainly on plasma density. The spectrogram in the top panel of Figure 1 demonstrates that in regions with low plasma density (with a decrease in f_{uhr}) there is AKR whose intensity decreases outside these regions (for example, at 17:02 UT). The dependence of the radiation intensity on the depth of the density dip is clearly seen at low frequencies ($f < 200$ – 250 kHz). At higher frequencies, radiation seeps out of the channel boundaries. The measurements were carried out in the evening local time. In this orbital period, the satellite, approaching Earth, moved from the dusk sector to the nightside magnetosphere — MLT varies from 18.7 to 19.2 hrs. In this region of the magnetosphere, P is not accurate since the plane in which the satellite's antennas rotate is almost perpendicular to the plane of AKR polarization. Nevertheless, the bottom panel of Figure 1 shows an increase in the P spectral intensity, which suggests that the processing results are sufficiently reliable. From this we can deduce that the source of the recorded AKR was in the Southern Hemisphere [Kolpak et al., 2021], while the satellite itself was in the Northern Hemisphere ($z > 0$).

At the beginning of the interval of interest, the plasma density was $\sim 100 \text{ cm}^{-3}$, and by the end of the interval it rose to $\sim 400 \text{ cm}^{-3}$. Such density variations indicate that the measurements were made at the outer boundary of the plasmapause as the satellite approached Earth. In the interval considered

$$f_{\text{hrp}2} / f_{\text{hrp}1} = 0.6 - 0.8,$$

where $f_{\text{hrp}2,1}$ are the upper hybrid resonance frequencies inside and outside the channel. This corresponds to

$$(N_1 - N_2) / N_1 = 0.36 - 0.64,$$

where N_1 is the background plasma density; N_2 is the density of plasma inside the channel. Thus, at a relative channel depth 0.36–0.64, radiation is captured at least at frequencies below 250 kHz.

Figure 2 shows that the AKR spectrum inside a channel

with low plasma density (solid line) is characterized by a rapid intensity increase at low frequencies and a relatively slow decrease at high frequencies, unlike the AKR spectrum in a homogeneous plasma (dashed line).

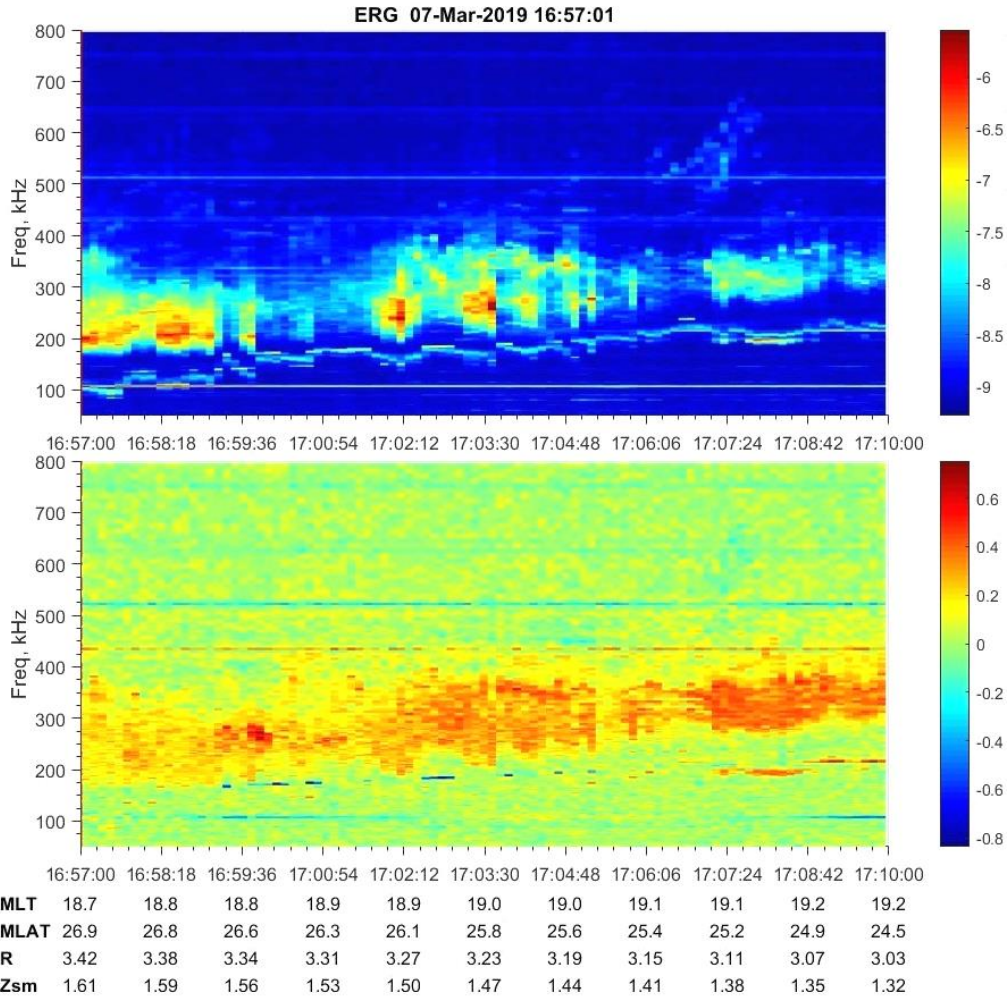


Figure 1. AKR in the region with channels with low plasma density from 16:57 to 17:10 UT on March 7, 2019 (results of HFA/PWE data processing): the top panel is a dynamic spectrogram of the strength of the electromagnetic field electric component in the frequency range 50–800 kHz; the bottom panel is a spectrogram of the polarization parameter P

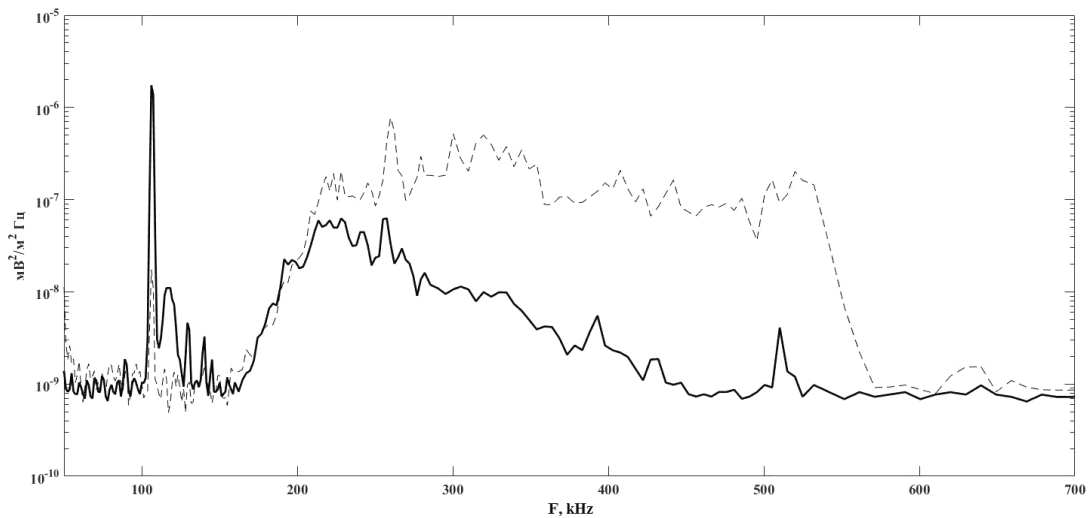


Figure 2. "Triangular" (solid line) and "flat" (dashed line) spectra of AKR detected at 16:56:05 UT on March 07, 2019 and at 19:44:51 UT on November 14, 2018 respectively

With an increase in frequency from ~ 170 to ~ 225 kHz (by 55 kHz), the intensity of the spectral components increases by two orders of magnitude; and with a further increase in frequency from ~ 225 kHz to ~ 450 kHz (by 225 kHz), it decreases by two orders of magnitude. This spectrum shape is peculiar to the AKR propagating in plasma channels [Mogilevsky et al., 2022]. An abrupt increase in the radiation intensity in the region of 100 kHz corresponds to oscillations at the upper hybrid resonance frequency.

Another example of AKR captured in plasma channels is given in Figure 3. Measurements were performed on December 19, 2018 from 09:15:00 to 11:00:00 UT. The satellite was in the dusk sector of the Southern Hemisphere ($z < 0$) and moved toward the nightside magnetosphere (MLT=17.3–18.2) in a direction away from Earth.

The top panel of Figure 3 shows a dynamic spectrogram of the strength of the electromagnetic field electric component in the frequency range 50–800 kHz. A narrowband signal in the frequency range of 75 to 175 kHz is electric field oscillations at the upper hybrid resonance frequency. As in Figure 2, measurements of the upper hybrid resonance frequency result from plasma density measurements, so in the first approximation we can assume that $f_{gr} \sim f_{pe}$. This means that the plasma density varies from 100 to 400 cm^{-3} over the time interval considered. The satellite might have crossed the plas-

mapause beyond the given time interval, but near it, at ~ 9 UT. Thus, the measurements were carried out at the outer boundary of the plasmasphere, which is also indicated by a gradual plasma density decrease with distance. At the beginning of the time interval, at 09:15–09:50 UT, the depth of density modulation is greater: $M = \Delta/N \sim 0.67$, and by the end of the interval it decreases to $M \sim 0.15$ – 0.25 . Transverse sizes of density dips also vary: at the beginning of the interval, the characteristic size of one lacuna is several hundred kilometers, and by the end of the interval it decreases to several tens of kilometers. The plasma density inside and outside the channel was calculated from the f_{uhr} measurements. At 10:24:51 UT, when the satellite was inside the channel, the plasma density was $N_2 \approx 157 \text{ cm}^{-3}$. Outside the channel, $N_1 \approx 164 \text{ cm}^{-3}$ behind the left wall and $N_1 \approx 161 \text{ cm}^{-3}$ behind the right wall.

The bottom panel of Figure 3 presents the P parameter spectrogram. Since the measurements were first made near the local evening time, i.e. the measured field component was almost perpendicular to the radiation polarization plane, P is zero. As the satellite moves toward the nightside magnetosphere, the P parameter changes and at 10:20 UT acquires a stable negative value, which indicates that the AKR source is located in the Northern Hemisphere. It is interesting to note that at $\sim 10:50$ UT there is radiation from another AKR source.

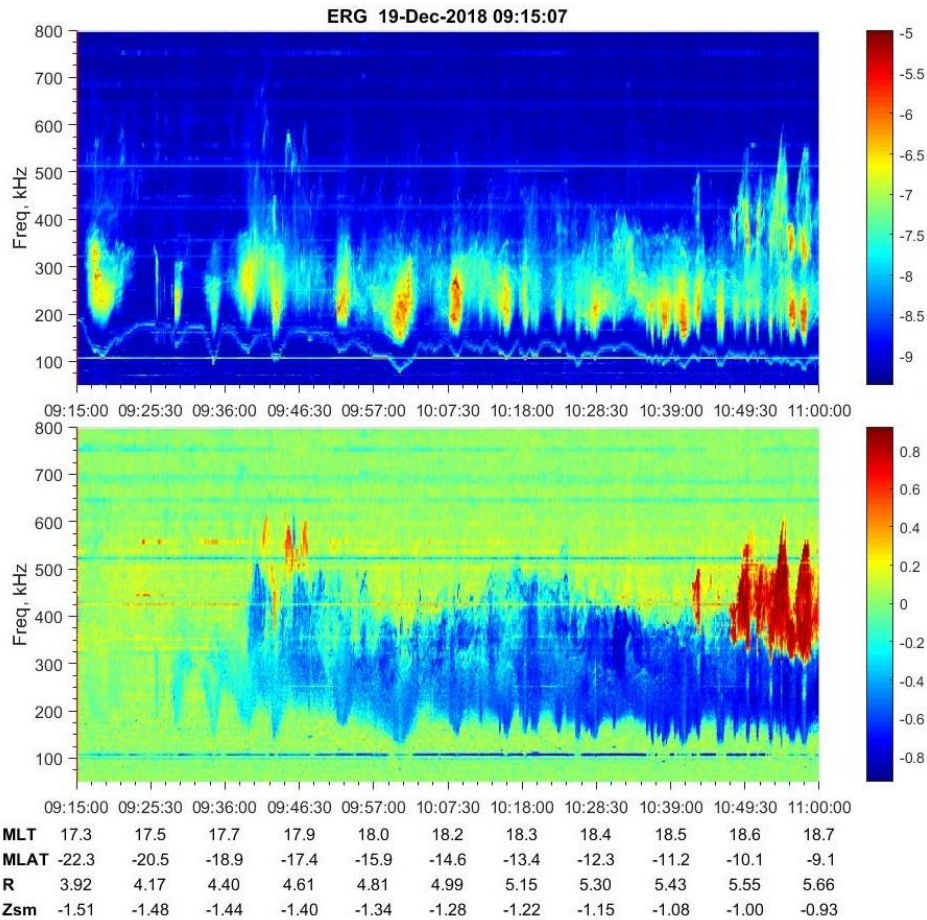


Figure 3. AKR in the region with channels with low plasma density on December 19, 2018 (the results are presented as in Figure 1)

This is clearly seen both in the dynamic spectrogram and in the P parameter spectrogram: the second source is higher-frequency ($\sim 300\text{--}500$ kHz) and has a positive P parameter, which suggests that it is located in the Southern Hemisphere.

The radiation spectrum from the two sources (December 19, 2018 at 10:53:31 UT) is a superposition of two triangular spectra (Figure 4). The top panel plots the frequency dependence of the radiation intensity. The sharp peak on the left corresponds to the upper hybrid resonance frequency. The AKR captured into the channel, in this case, has a spectrum with two humps. The bottom panel plots the P parameter of this radiation. In the frequency range 170–320 kHz, the P parameter is negative, and at 320–510 kHz it is positive. Hence it follows that radiation from two sources located in different hemispheres is observed in one channel.

From the results of ERG (Arase) electromagnetic field measurement processing we can deduce that there is an AKR captured into plasma channels, or lacunae, — regions with low plasma density. It follows from the sign of the parameter P that the AKR in the equatorial region can be generated by sources located in both the Northern and Southern hemispheres. It is logical to assume that the observed plasma inhomogeneities are

elongated along the magnetic field at the outer boundary of the plasmopause and comprise channels. Dimensions of these channels across the magnetic field are much larger than the AKR wavelength, which makes it possible to simulate the capture of radiation into the channel and propagation in it in the geometrical optics approximation.

DISCUSSION OF MEASUREMENT RESULTS AND MODELING OF CONDITIONS FOR AKR CAPTURE AND PROPAGATION

Calculations have been performed to assess the conditions for radiation capture into a channel and propagation in it. We used the following simplifications:

- it is believed that the walls of the channels are sharp, i.e. the density changes abruptly from N_1 to N_2 ;
- it is thought that the walls of the channel are parallel, i.e. the channel does not expand along the magnetic field and has the same dimensions along its entire length;
- a two-dimensional problem is considered without taking into account the effects caused by different channel cross-sections;

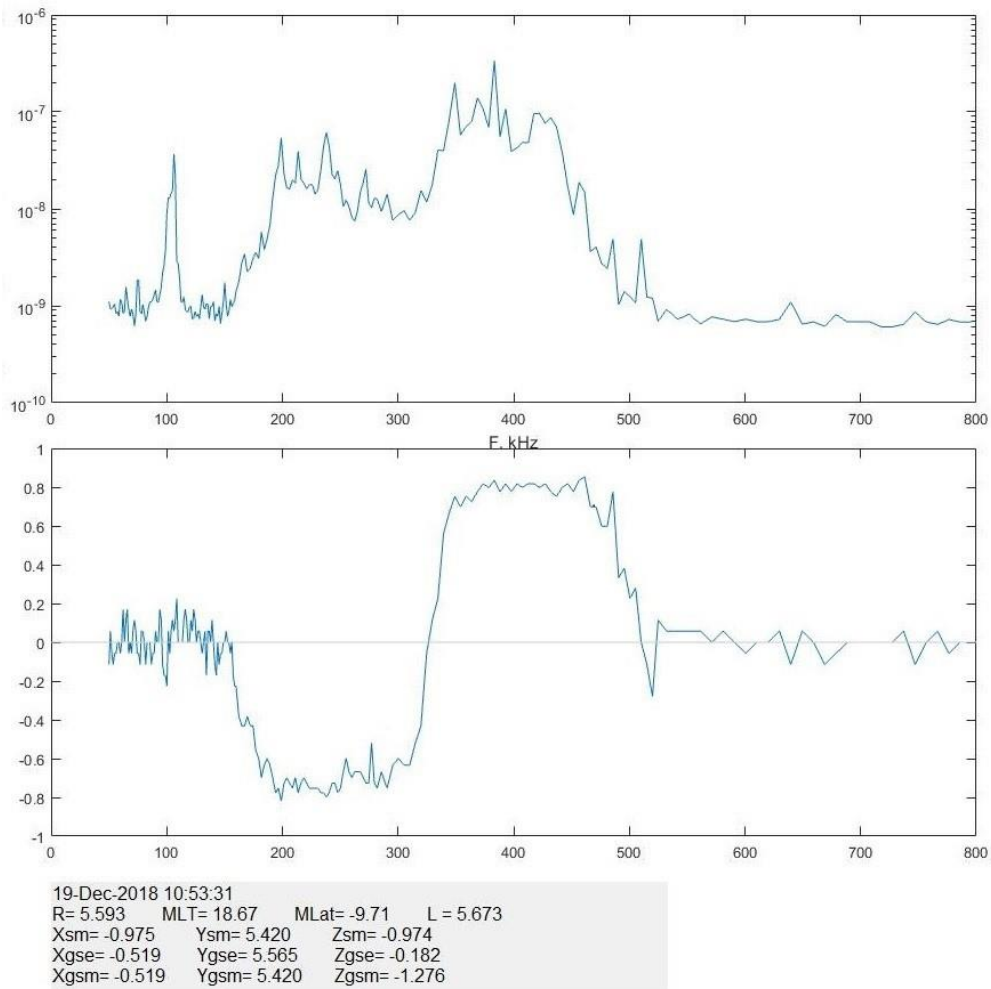


Figure 4. Spectrum of AKR from two sources located in different hemispheres: the top panel is the frequency dependence of the radiation intensity; the bottom panel is the P parameter

- it is neglected that the channel should bend in the same way as the geomagnetic field lines since it tracks them;
- the channel is assumed to be continuous and stationary.

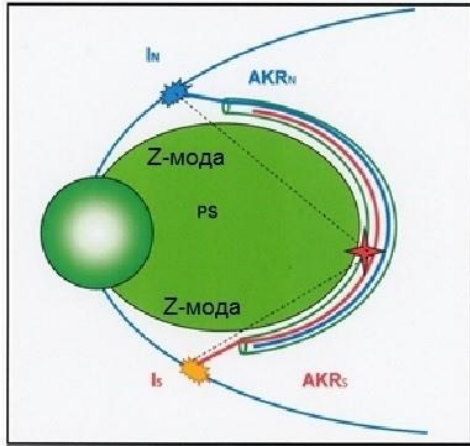
Despite the simplifications, the calculations, as shown below, give a qualitatively correct picture of AKR distribution in the channel.

Figure 5 on the right shows a scheme for capturing radiation into the channel and its propagation from the source in the auroral field line. The radiation enters the plasma channel near the plasmopause located closer to the equator of the source. Vertical lines are the walls of the channel; the arrow is the radiation captured into the channel; the horizontal dashed line is the length of one jump during propagation; inclined dashed lines are the radiation seeping out through the walls of the channel.

In all experiments with radiation capture, the plasma density in the channels was lower than the background values. Accordingly, in modeling we assume that the plasma density inside the channel is lower than outside it ($N_2 < N_1$ in Figure 5). The radiation angle of incidence onto the channel wall (and its reflection) is designated as θ_1 ; the radiation angle of refraction, as θ_2 .

The geometrical optics approximation was used to calculate radiation propagation in the channel. For a single reflection from the channel wall, we apply the well-known expressions for the reflection coefficient K and the transmission coefficient T [Landsberg, 2003]:

$$K = \left(\frac{n_2 \cos \theta_2 - n_1 \cos \theta_1}{n_2 \cos \theta_2 + n_1 \cos \theta_1} \right)^2, \quad (3)$$



where n_1 and n_2 are the refractive indices outside and inside the channel respectively; θ_1 and θ_2 are the incidence and refraction angles; $n_{1,2}^2 = 1 - \frac{\omega_{pe1,2}^2}{(\omega - \omega_{He} \cos \theta_{1,2}) \omega}$ is the refractive index for an extraordinary electromagnetic wave in plasma;

$$T = 1 - K. \quad (4)$$

Numbers in Figure 5 indicate: 1 — I_0 , radiation captured into the channel; 2 — $I_0 T$, where T is the transmission coefficient; 3 — $I_0 K$, where K is the reflection coefficient; 4 — $I_0 K^2$.

Figure 6 presents the results of calculations of the incidence angle dependence of the reflection coefficients for the minimum (167.2 kHz, top panel) and maximum (500 kHz, bottom panel) frequencies in the spectrum (see Figure 3). The calculations were carried out for the plasma density N_2 of 157, 120, and 80 cm^{-3} inside the channel, which is consistent with the values obtained in the experiment. The background plasma density outside the channel $N_1 = 160 \text{ cm}^{-3}$, which also agrees with the measurement results.

The calculation results suggest that the reflection coefficient K depends strongly on the angle of incidence. When the critical angle of incidence is reached (see below), K becomes equal to 1 and does not change with a

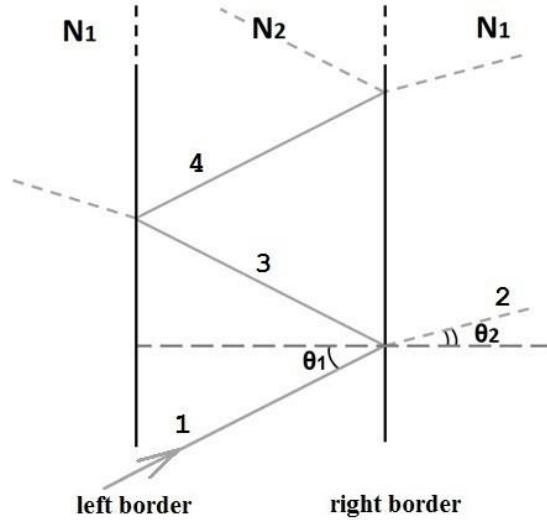


Figure 5. Mechanism of radiation transfer from one hemisphere to another by plasma inhomogeneities (left) and a scheme of radiation propagation in the channel (right)

Table 1

| Critical angles of incidence of radiation onto channel walls | | Critical angles for frequency | |
|--|-------------------|-------------------------------|-----------|
| Density N_2, cm^{-3} | $(N_1 - N_2)/N_1$ | 167.2 kHz | 500.2 kHz |
| 80 | 0.5 | 56.5° | 80.5° |
| 120 | 0.75 | 64.9° | 83.3° |
| 157 | 0.98 | 82.7° | 88.1° |

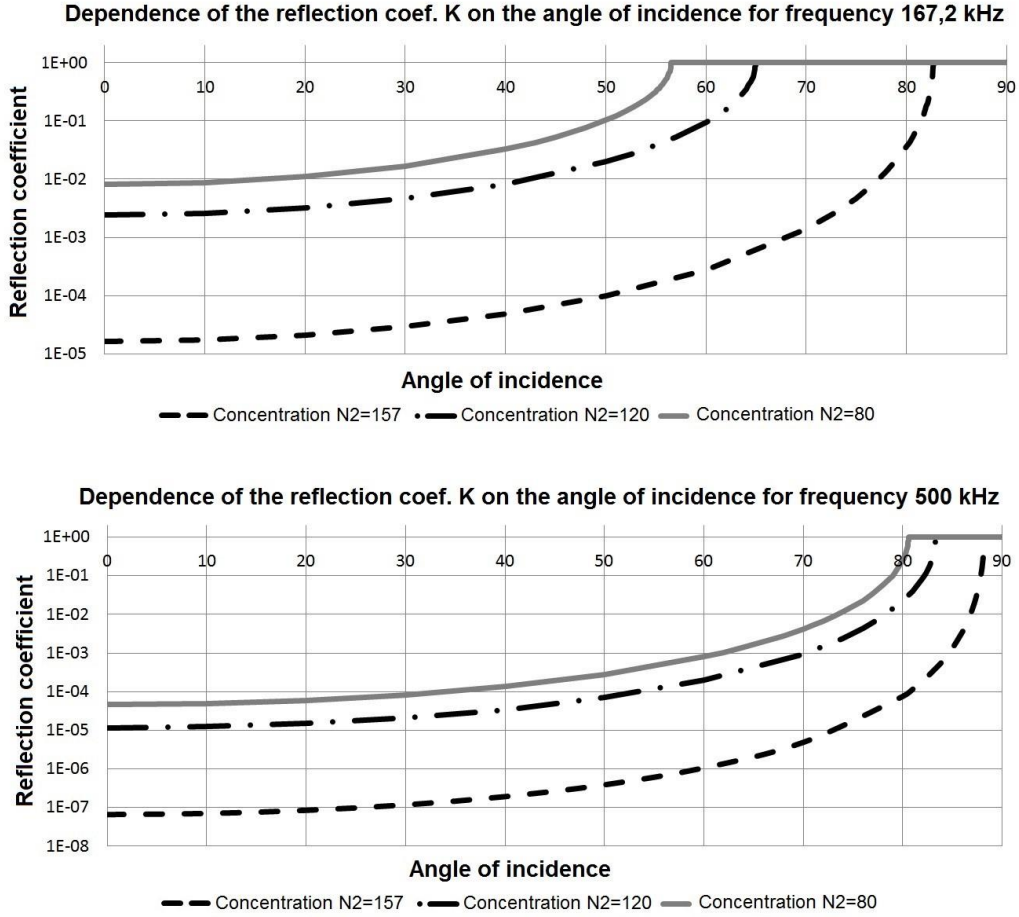


Figure 6. Reflection coefficient (on a logarithmic scale along the vertical axis) as a function of the angle of incidence for frequencies of 167.2 kHz (top panel) and 500 kHz (bottom panel)

further increase in the angle of incidence. This means that at angles greater than the critical one, radiation can propagate in the channel without losses caused by its seepage through the channel walls.

Limitations on the angle of incidence (Figure 6) are shown in Table 1. At angles less than critical ones (see Table), the radiation does not propagate in the channel.

When a signal is reflected multiple times from the channel walls, $K_m = K_1^m$, where m is the number of reflections of the signal from the channel walls. To estimate the number of reflections, we have employed the dipole field line approximation [Roederer, 1972]

$$dS = r_0 \cos \varphi \sqrt{4 - 3 \cos^2 \varphi} d\varphi, \quad (5)$$

where $\frac{r_0}{R_E} = L$; r_0 is the distance to the equatorial point

of the field line (maximum distance from Earth); R_E is the Earth radius; φ is the magnetic latitude of the tube (the beginning of the channel with a reduced plasma density); φ_0 is the magnetic latitude of the satellite:

$$\varphi_0 = \arccos \sqrt{\frac{1}{L}}, \quad L = \frac{1}{\cos^2 \varphi_0}. \quad (6)$$

In this approximation, the length of the field line segment

$$S = \frac{3L \sin \varphi_0 \sqrt{3 \sin \varphi_0 + 1} + \sqrt{3} L \ln \left| \sqrt{3 \sin \varphi_0 + \sqrt{3 \sin^2 \varphi_0}} \right|}{6} + \frac{3L \sin \varphi \sqrt{3 \sin \varphi + 1} + \sqrt{3} L \ln \left| \sqrt{3 \sin \varphi + \sqrt{3 \sin^2 \varphi}} \right|}{6}. \quad (7)$$

From the experiment, we determine the length of one jump ($\Delta R \operatorname{tg} \theta_1$).

Using the estimated jump length and length of the field line segment, we can determine the number of radiation jumps during its propagation in the channel: 30–100.

At such values of m , K_m as the angle of incidence approaches the critical one increases faster than shown in Figure 6. Thus, the critical angles listed in Table 1 define the angular dependence of the decrease in the reflection coefficients: the smaller the angles at which the radiation is captured into the channel, the less flat is the plot.

Figure 7 presents the results of calculations of K as a function of frequency for 85° , 80° , and 75° angles of incidence onto the channel wall. The calculations were performed for frequencies exceeding the frequency of the maximum spectrum obtained in the experiment. All three plots indicate that with an increase in frequency by 150–250 kHz, K decreases by two orders of magnitude, which is in good agreement with the measurement results (see Figure 2).

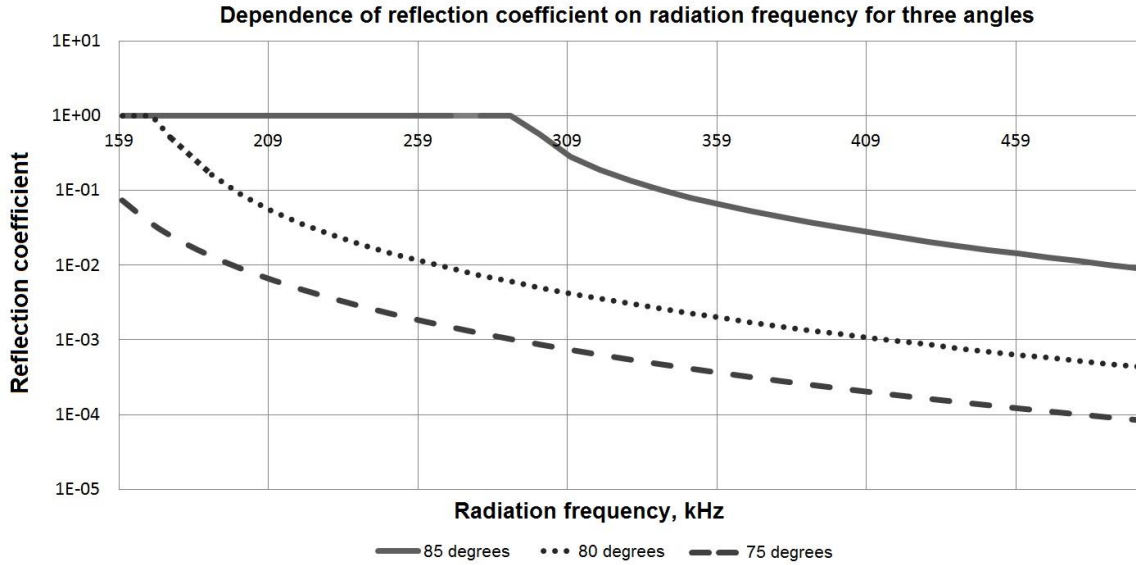


Figure 7. Reflection coefficient as a function of frequency for three angles of incidence onto the channel wall at $N_1=164 \text{ cm}^{-3}$ and $N_2=157 \text{ cm}^{-3}$

We have analyzed the relative position of the AKR source and the channel into which the radiation can be captured. The position of the channels was determined from ERG satellite (Arase) data. Radiation angles of incidence onto the channel wall were calculated from the dipole geometry. The calculations have been made for three positions of the AKR source: the magnetic field line of the source at $\varphi_l=68^\circ, 70^\circ,$ and 75° of invariant latitude. The height of the source (the distance from Earth's surface to the point of radiation) was found using a dipole field model, taking into account that AKR is generated near the local electron gyrofrequency.

Figure 8 provides an example of calculations for the 68° AKR invariant latitude of the source field line. The following designations are used: 1 — AKR source position; 2 — position of the lower boundary of radiation capture into the channel ($\varphi=50.6^\circ, R=2.19$); 3 — tangent to the channel field line drawn from the source ($\varphi=44.6^\circ, R=2.75$); A — tangent to the field line in source 1; B — the magnetic field line on which the AKR source is located; C — the magnetic field line on which the channel is located. Distance in Earth radii is plotted along the axes. The dashed line from AKR source 1 to the field line of channel 3 is tangent to the field line of the source. The angle between the tangent to the source field line and the tangent to the channel field line is the minimum angle at which radiation coming from the source can enter the plasma channel. The solid line coming from the source and crossing the channel field line at point 2 is the maximum angle at which radiation can propagate in the channel without damping (see Figure 6).

We have calculated the length of the magnetic field line segment (the distance between points 2 and 3 in Figure 8 is equal to ΔR) at which the channel inlet can be located. The calculation results (in Earth radii) are shown in Table 2. According to [Mogilevsky et al., 2007], the radiation cone opening is $\pm(25^\circ-35^\circ)$. Values that meet these limitations are marked with an asterisk.

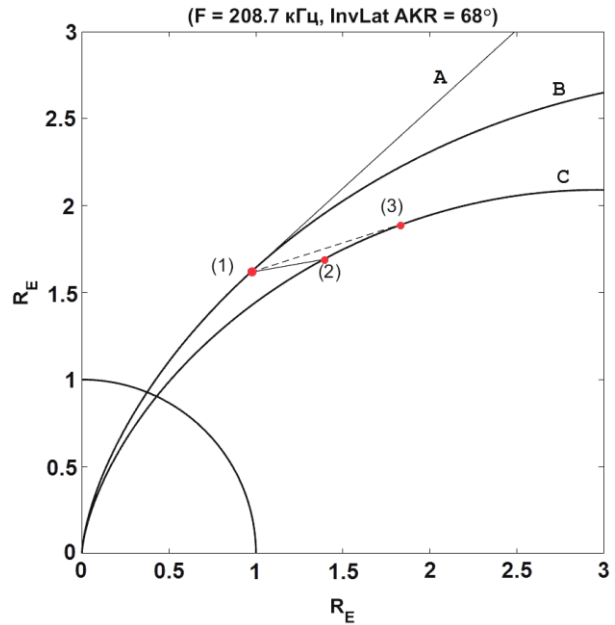


Figure 8. Results of calculation of the relative position of AKR source (1) and magnetic field line (2) on which the plasma channel is located (according to the measurement results obtained on December 19, 2018). Designations — see the text

Table 2
Results of calculations of the length of magnetic field line segment (in Earth radii)

| | Invar. lat. | 68° | 70° | 75° |
|-----------|-------------|------------|------------|------------|
| Frequency | | | | |
| 167.2 kHz | | 0.67* | 0.75 | 0.85 |
| 208.7 kHz | | 0.56* | 0.63* | 0.69 |
| 500.2 kHz | | 0.27* | 0.30* | 0.31 |

Analysis of the calculation results shows that in order to capture AKR into the channel, its source should be near the channel (the invariant latitude of the magnetic field line with AKR $\varphi_l \approx 68^\circ-70^\circ$). We can roughly

assess the probability of detecting AKR captured into the plasma channel:

$$W \approx 2\Delta R / L \approx 0.1 - 0.2. \quad (8)$$

The estimated values of W are close in order of magnitude to the measurement results — when observed continuously, the AKR capture is detected several times a month.

CONCLUSIONS

From ERG (Arase) satellite measurement results and calculations, we have found that auroral radiation can be transferred from one hemisphere to another. The following has been established:

- when propagating in channels, the higher-frequency part of AKR ($f > 300$ – 400 kHz) seeps out the channels to a greater extent than the low-frequency one ($f < 300$ – 400 kHz);
- when radiation propagates in the channels, the AKR spectrum is transformed: a rapid decrease in the intensity of spectrum components at low frequencies ($f < 150$ – 200 kHz) and a relatively slow decrease at high frequencies ($f > 150$ – 200 kHz);
- the results of modeling of AKR propagation in plasma channels agree with the measurements quite well and explain the AKR spectrum transformation (from ~ 200 kHz to ~ 400 kHz, the intensity decreases by two orders of magnitude);
- from analysis of the conditions for the AKR capture into plasma channels it follows: the capture depends on the relative position of the source and the channel, as well as on the depth of the plasma density dip inside the channel ($\Delta N/N$).

Thus we have confirmed the results of ISEE-1 satellite measurements indicating the possibility of capturing AKR into channels formed near the plasmopause by plasma inhomogeneities elongated along the magnetic field.

We express our thanks to A. Kumamoto, Y. Kasahara, F. Tsuchiya for providing PWE/HFA-L2 v01.01 data [Kasahara et al., 2018; Kumamoto et al., 2018]. The ERG (Arase) satellite data, as well as the description and characteristics of scientific instruments, were obtained from the ERG (Arase) Science Center, operated by ISAS/JAXA and ISEE/Nagoya University, on the website [<https://ergsc.isee.nagoya-u.ac.jp/>] [Miyoshi et al., 2018a, b].

The work of V.I. Kolpak and A.A. Chernyshov was financially supported by the Foundation for the Development of Theoretical Physics and Mathematics “BASIS”.

REFERENCES

Baumjohann W., Treumann R.A. Auroral kilometric radiation — the electron cyclotron maser paradigm. *Front. Astron. Space Sci.* 2022, vol. 9, 1053303. DOI: [10.3389/fspas.2022.1053303](https://doi.org/10.3389/fspas.2022.1053303).

Benediktov E.A., Getmancev G.G., Mitjakov N.A., Rapoport V.A., Sazonov Ju.A., Tarasov A.F. Results of measuring the intensity of radio emission at 725 and 1525 kHz frequencies using the equipment installed on “ELECTRON-2” satellite. *Issledovaniya kosmicheskogo prostranstva* [Space

exploration]. Moscow, Nauka Publ., 1965, pp. 581–606. (In Russian).

Burinskaya T.M., Rosh Zh.L. Waveguide regime of cyclotron maser instability in plasma regions with reduced density. *Fizika plazmy* [Plasma Phys.]. 2007, vol. 33, no. 1, pp. 28–37 (In Russian).

Calvert W. Ducted auroral kilometric radiation. *Geophys. Res. Lett.* 1982, vol. 9, no. 1, pp. 56–59. DOI: [10.1029/GL009i001p00056](https://doi.org/10.1029/GL009i001p00056).

Chernyshov A.A., Chugunin D.V., Mogilevsky M.M. Auroral kilometric radiation as a diagnostic tool for the properties of the magnetosphere. *JETP Lett.* 2022a, vol. 115, pp. 23–28. DOI: [10.1134/S0021364022010076](https://doi.org/10.1134/S0021364022010076).

Chernyshov A.A., Mogilevsky M.M., Chugunin D.V., Kolpak V.I. Simultaneous observation of auroral kilometric radiation from northern and southern sources. *Bulletin of the Russian Academy of Sciences: Physics.* 2022b, vol. 86, no. 3, pp. 295–299. DOI: [10.3103/S1062873822030078](https://doi.org/10.3103/S1062873822030078).

Chugunin D.V., Chernyshov A.A., Moiseenko I.L., Mogilevsky M.M., Viktorov M.E. Monitoring of the electron-acceleration region with auroral kilometric radiation. *Geomagnetism and Aeronomy.* 2020, vol. 60, no. 5, pp. 538–546. DOI: [10.1134/S0016793220040039](https://doi.org/10.1134/S0016793220040039).

Gurnett D.A. The Earth as a radio source: Terrestrial kilometric radiation. *J. Geophys. Res.* 1974, vol. 79, no. 28, pp. 4227–4238. DOI: [10.1029/JA079i028p04227](https://doi.org/10.1029/JA079i028p04227).

Hanasz J., Panchenko M., De Feraudy H., Schreiber R., Mogilevsky M.M. Occurrence distributions of the auroral kilometric radiation ordinary and extraordinary wave modes. *J. Geophys. Res.* 2003, vol. 108, no. A11, 1408. DOI: [10.1029/2002JA009579](https://doi.org/10.1029/2002JA009579).

Kolpak V.I., Mogilevsky M.M., Chugunin D.V., Chernyshov A.A., Moiseenko I.L., Kumamoto A., Tsuchiya F., et al. Statistical properties of auroral kilometer radiation: based on ERG (Arase) satellite data. *Solar-Terr. Phys.* 2021, vol. 7, iss. 1, pp. 11–16. DOI: [10.12737/stp-71202102](https://doi.org/10.12737/stp-71202102).

Kasahara Y., Kasaba Y., Kojima H., Yagitani S., Ishisaka K., Kumamoto A., et al. The Plasma Wave Experiment (PWE) on board the Arase (ERG) satellite. *Earth, Planets and Space.* 2018, vol. 70, 86 p. DOI: [10.1186/s40623-018-0842-4](https://doi.org/10.1186/s40623-018-0842-4).

Kumamoto A., Tsuchiya F., Kasahara Y., Kasaba Y., Kojima H., Yagitani S., et al. High Frequency Analyzer (HFA) of Plasma Wave Experiment (PWE) onboard the Arase spacecraft. *Earth, Planets and Space.* 2018, vol. 70, 82 p. DOI: [10.1186/s40623-018-0854-0](https://doi.org/10.1186/s40623-018-0854-0).

Kurth W.S., Baumbach M.M., Gurnett D.A. Direction-finding measurements of auroral kilometric radiation. *J. Geophys. Res.* 1975, vol. 80, no. 19, p. 2764.

Landsberg G.S. *Optica: ucheb. posobie dlya vuzov* [Optics: Tutorial]. Moscow, Fizmatlit Publ., 2003, 848 p. (In Russian).

Louarn P., Le Quéau D. Generation of the auroral kilometric radiation in plasma cavities. II. The cyclotron maser instability in small size sources. *Planet. Space Sci.* 1996, vol. 44, no. 3, pp. 211–224. DOI: [10.1016/0032-0633\(95\)00122-0](https://doi.org/10.1016/0032-0633(95)00122-0).

Miyoshi Y., Shinohara I., Takashima T., Asamura K., Higashio N., Mitani T., Kasahara S., Yokota S., Kazama Y., et al. Geospace Exploration Project ERG. *Earth, Planets and Space.* 2018a, vol. 70, 155 p. DOI: [10.1186/s40623-018-0862-0](https://doi.org/10.1186/s40623-018-0862-0).

Miyoshi Y., Hori T., Shoji M., Teramoto M., Chang T.F., Segawa T., Umemura N., Matsuda S., Kurita S. The ERG Science Center. *Earth, Planets and Space.* 2018b, vol. 70, 96. DOI: [10.1186/s40623-018-0867-8](https://doi.org/10.1186/s40623-018-0867-8).

Mogilevsky M.M., Romancova T.V., Hanash Ja., Burinskaja T.M., Shrajber R. About the source of auroral kilometric radiation. *Pis'ma v ZhETF* [J. Experimental and Theoretical Phys. Lett.]. 2007, vol. 86, iss. 11, pp. 819–821. (In Russian).

Mogilevsky M.M., Chugunin D.V., Chernyshov A.A., et al. Channeling of auroral kilometric radiation during geomag-

netic disturbances. *JETP Lett.* 2022, vol. 115, pp. 602–607. DOI: [10.1134/S0021364022600707](https://doi.org/10.1134/S0021364022600707).

Nagai T., Mauk B., Santolik O., Kubota T., Sakanoi T. Special issue “Geospace exploration by the ERG mission”. *Earth, Planets and Space.* 2018, vol. 70, 155. DOI: [10.1186/s40623-018-0926-1](https://doi.org/10.1186/s40623-018-0926-1).

Roederer J.G. *Dynamics of Geomagnetically Trapped Radiation.* Springer-Verlag Berlin Heidelberg, 1970, 166 p. (Physics and Chemistry in Space, vol. 2). DOI: [10.1007/978-3-642-49300-3](https://doi.org/10.1007/978-3-642-49300-3).

Wu C.S. The cyclotron maser theory of AKR and Z-mode radiation. *CNES Results of the ARCAD 3 Project and of Recent Programs in Magnetospheric and Ionospheric Physics.* 1985, pp. 559–570.

Wu C.S., Lee L.C. A theory of the terrestrial kilometric radiation. *Astrophys. J.* 1979, vol. 230, pp. 621–626.

Xiao F., Tang J., Zhang S., Zhou Q., Liu S., He Y., et al. Asymmetric distributions of auroral kilometric radiation in Earth’s Northern and Southern hemispheres observed by the Arase satellite. *Geophys. Res. Lett.* 2022, vol. 49, no. 13, e2022GL099571. DOI: [10.1029/2022GL099571](https://doi.org/10.1029/2022GL099571).

Zhao W., Liu S., Zhang S., Zhou Q., Yang C., He Y. Global occurrences of auroral kilometric radiation related to suprathermal electrons in radiation belts. *Geophys. Res. Lett.* 2019, vol. 46, no. 10, pp. 7230–7236. DOI: [10.1029/2019GL083944](https://doi.org/10.1029/2019GL083944).

URL: <https://ergsc.isee.nagoya-u.ac.jp/> (accessed September 12, 2023).

Original Russian version: Kolpak V.I., Mogilevsky M.M., Chuginin D.V., Chernyshov A.A., Moiseenko I.L., published in *Solnechnozemnaya fizika.* 2024. Vol. 10. Iss. 1. P. 21–30. DOI: [10.12737/szf-101202403](https://doi.org/10.12737/szf-101202403). © 2023 INFRA-M Academic Publishing House (Nauchno-Izdatelskii Tsentr INFRA-M)

How to cite this article

Kolpak V.I., Mogilevsky M.M., Chuginin D.V., Chernyshov A.A., Moiseenko I.L. Transfer of auroral kilometric radiation through low-density channels at the boundary of plasmasphere. *Solar-Terrestrial Physics.* 2024. Vol. 10. Iss. 1. P. 19–28. DOI: [10.12737/stp-101202403](https://doi.org/10.12737/stp-101202403).